Sensors & Actuators: B. Chemical 446 (2026) 138652

Contents lists available at ScienceDirect

Sensors and Actuators: B. Chemical

journal homepage: www.elsevier.com/locate/snb

Piezoelectric tuning forks employed as photodetectors for hydrogen sensing

Mariagrazia Olivieri [a], Giansergio Menduni [a,b,*], Andrea Zifarelli [a,b], Aldo F.P. Cantatore [a], Marilena Giglio [a], Huseyin R. Seren [c], Miguel Gonzalez [c,**], Huadan Zheng [d], Hongpeng Wu [a,e,f], Lei Dong [a,e,f], Pan Luo [g], Pietro Patimisco [a,b], Vincenzo Spagnolo [a,b], Angelo Sampaolo [a,b]

[a] PolySense Lab, Dipartimento Interateneo di Fisica M. Merlin, Università degli Studi di Bari Aldo Moro e Politecnico di Bari, Via G. Amendola 173, Bari 70125, Italy
[b] PolySense Innovations srl, Via Amendola 173, Bari 70126, Italy
[c] Aramco Services Company, Park Row 17155, Houston, TX 77084, USA
[d] Guangdong Provincial Key Laboratory of Optical Fiber Sensing and Communications, and Department of Optoelectronic Engineering, Jinan University, Guangzhou 510632, PR China
[e] State Key Laboratory of Quantum Optics and Quantum Optics Devices, Institute of Laser Spectroscopy, Shanxi University, Taiyuan 030006, PR China
[f] Collaborative Innovation Center of Extreme Optics, Shanxi University, Taiyuan 030006, PR China
[g] EXPEC Advanced Research Center, Saudi Aramco, Dhahran 31311, Saudi Arabia

ARTICLE INFO

Keywords:
Hydrogen
Multi-pass cell
LITES
Quartz
Lithium niobate

ABSTRACT

A study on the H_2 spectral properties and a comparison between two different piezoelectric resonators employed as infrared detectors for hydrogen sensing are reported. A quartz tuning fork (QTF) and a lithium niobate tuning fork (LiNTF) are implemented in the same light-induced thermoelastic spectroscopy experimental set-up, employing i) a laser diode to target the hydrogen absorption feature at 4712.90 cm^{-1}, characterized by low interference from other contaminants; ii) a multi-pass cell with a 10.4 m pathlength, to enhance the interaction between light and H_2 molecules. Both resonators demonstrate a linear response with respect to the hydrogen concentration and a minimum detection limit (MDL) of 0.50 % and of 1.50 % at 0.1 s of integration time with the QTF and the LiNTF, respectively. The long-term stability analysis highlights a bias instability for the QTF, mainly addressed to the inhomogeneities at the edge of the active area. Conversely, the uniform surface of the LiNTF returns a highly stable detection, allowing an MDL as low as 0.1 % at 64 s of integration time. This first demonstration of a LiNTF as photodetector paves the way to the realization of fully integrated sensors based on lithium-niobate-on-insulator platforms.

1. Introduction

Hydrogen is expected to play an important role in the global energy transition towards a low-carbon future. For example, in addition to the chemical, power, and transportation industries, its use is being explored in key heavy industrial sectors that are difficult to decarbonize, such as the stainless-steel industry and cement industries [1,2]. Production, storage and distribution of hydrogen can take different paths within the hydrogen value chain, as multiple sources (e.g. electrolysis, steam methane reforming with carbon capture, nuclear, etc.), modes of transportation (e.g. ammonia, liquid organic hydrogen carriers, cryogenic/cryo-compressed gas etc.), storage technologies (e.g. geologic, material-based storage, etc.), and end-uses (e.g. transportation, power, chemical industries, etc.) are considered. Thus, the infrastructure required to effectively deploy hydrogen as a commercially viable energy carrier or feedstock can be quite complex and will necessitate novel hydrogen gas monitoring technologies at each step, from generation/production to end-use. It is worth mentioning combustion properties of hydrogen, i.e., low minimum ignition energy (0.017 mJ), high heat of combustion (142 kJ/g), wide flammable range (4-75 %) and high burning velocity [3]. These pose challenges for the safety and handling of hydrogen at large scales. These properties also determine the calorific value of natural gas and hydrogen blends, as proposed vector for hydrogen distribution and combustion [4]. A lot of research is currently focused on H_2 production and storage processes to fully exploit its potential as a resource for the energy industry and to

* Corresponding author at: PolySense Lab, Dipartimento Interateneo di Fisica M. Merlin, Università degli Studi di Bari Aldo Moro e Politecnico di Bari, Via G. Amendola 173, Bari 70125, Italy.
** Corresponding author.
E-mail addresses: giansergio.menduni@poliba.it (G. Menduni), miguel.gonzalez@aramcoamericas.com (M. Gonzalez).

https://doi.org/10.1016/j.snb.2025.138652
Received 4 May 2025; Received in revised form 28 August 2025; Accepted 31 August 2025
Available online 2 September 2025

allow an integration into different sectors [5]. Therefore, the monitoring of H_2 concentration can help improving the efficiency of these processes. More recently, the possibility to produce naturally occurring hydrogen from geological formations has attracted a lot of attention [6]. New hydrogen sensing technologies are emerging as valuable tools for detecting hydrogen seepage in surface geochemical surveys and explore subsurface hydrogen accumulations during drilling programs in petroleum exploration. The hydrogen sensor deployed in the field may also aid in-situ measurement of hydrogen concentration in different fluids and monitoring hydrogen production rates to utilize this tantalizing hydrogen source [7].

Several types of hydrogen sensors have been commercialized thus far, e.g., catalytic sensors, electrochemical sensors, metal oxide sensors; however, their working principle is based on the alteration of the sensing element when interacting with H_2 in gas phase [1–3], thus preventing the use in corrosive, reactive and dusty gas streams. Optical sensors represent an effective alternative for H_2 detection, since they allow non-contact measurements, as in tunable diode laser absorption spectroscopy (TDLAS) [4–6]. In this technique, the emission wavelength of a laser source is scanned across the selected gas absorption line and the residual light is acquired and converted in an electric signal by a photodetector [7]. In TDLAS, the detector could be placed outside the gas chamber, thus not affecting and altering the detection properties of the sensitive element [8–10]. Avetisov et al. (2019) reported for the first time on a sensor based on TDLAS for in-situ hydrogen measurements in a non-contact configuration [11]. Being a diatomic homonuclear molecule, H_2 does not possess a permanent dipole moment and therefore its absorption spectrum in the infrared spectral range is limited to very weak and sparse absorption lines corresponding to electrical quadrupole transitions, with the fundamental ones localized within the range 1900–3000 nm [12,13]. The implementation of multi-pass cell (MPC) in a TDLAS set-up increases the interaction pathlength between light and the gas molecules, thus allowing the detection of the H_2 weak absorption features [14–17]. Considering the possible applications of H_2 sensing, the selection of the absorption peak must consider both the value of the linestrength and the possible interfering components. As reported in Avetisov et al. (2019) [11], the peak centered at 4712.90 cm^{-1} (2121.84 nm) should be selected for optical sensing since it provides both the highest linestrength ($3.18 \cdot 10^{-26}$ cm/molecule, [18]) and the lowest interference from other possible contaminants, such as water vapor (H_2O), carbon dioxide (CO_2), methane (CH_4), ammonia (NH_3), and carbon monoxide (CO), typically present in industrial processes [11, 18,19]. In a TDLAS sensor, the achievable detection limit is mainly determined by the properties of the employed photodetector [20,21]. Recently, quartz tuning forks (QTFs) have been employed as light detectors in TDLAS experiments, resulting in the novel approach known as light-induced thermoelastic spectroscopy (LITES) [22–27]. In this technique, the portion of light absorbed by the QTF generates through thermoelastic conversion a deformation, corresponding to an electric signal due to the piezoelectricity of quartz [28]. Yufei Ma et al. employed a quartz tuning fork with a resonance frequency f∼30 kHz and quality factor Q∼8500 for detecting H_2 absorption feature [29]. They enhanced sensitivity through two approaches: implementing a multi-pass cell to extend the interaction pathlength and developing a neural network-based denoising algorithm. The denoising approach reduced the noise by two orders of magnitude, improving the sensor minimum detection limit (MDL) from thousands of parts per million (ppm) to tens of ppm. Nevertheless, the main challenge remains to achieve high sensitivity and selectivity in direct absorption techniques while maintaining a simple, fast, compact, robust and cost-effective sensor architecture: a balance that requires careful optimization of competing factors.

In this work, we extensively investigate both the peculiarity of the molecular H_2 optical excitation and the characteristics of different possible detectors, having as final goal the design of a potential versatile and robust H_2 analyzer, easily convertible for detection of other related target molecules. A detailed study on the H_2 spectral properties is reported, employing a standard photodetector and, thereafter, two different piezoelectric tuning forks have been employed for hydrogen sensing in the same LITES experimental set-up: a QTF resonating at 9.8 kHz [24] and a lithium niobate tuning fork (LiNTF), having a resonance frequency of 40 kHz. This last type of resonators have been widely used as sensitive elements (e.g., assessment of fluid characteristics [30–32], photoacoustic spectroscopy [33]), but LiNTF is reported here for the first time as light detector, in particular for H_2 sensing. Finally, MDL and the stability of both the QTF and the LiNTF in the same experimental set-up are discussed.

The special focus on the introduction of a LiNTF mechanical resonator employed as photodetector is due to the fact that, in the perspective of all-integrated on-chip sensing platforms, this crystal offers significant advantages over quartz-based piezoelectric detectors in terms of miniaturization potential and compatibility with modern semiconductor fabrication processes. Significant advantages are also offered in terms of electromechanical coupling. With respect to the quartz crystal, the effective piezoelectric coefficient of 128° y-cut lithium niobate, the only one involved in the excitation of the fundamental in-plane anti-symmetric flexural mode, is nearly 10 times higher than that of α-quartz (2–3 pC/N) [34,35]. Moreover, lithium niobate has higher density and Young's modulus (4650 kg/m^3 and 145 GPa, respectively) with respect to quartz (2660 kg/m^3 and 72 GPa). Furthermore, the high acoustic velocity (∼7000 m/s) in LiN supports the design of high-frequency devices, essential for enhanced temporal resolution and improved selectivity in complex environments [36]. The ability to integrate these resonators directly on a chip allows for compact, scalable systems that are compatible with CMOS technologies, facilitating seamless integration with electronic signal processing circuits. Additionally, the anisotropic properties of lithium niobate enable engineers to exploit specific crystallographic orientations to optimize device performance for target applications. In contrast, quartz resonators, although widely used, are limited by their relatively lower electromechanical coupling and challenges in miniaturization due to bulk fabrication techniques, which hinder their scalability for advanced multi-sensor arrays or lab-on-chip systems.

Therefore, the main goal and innovation aspect of this work consist in unlocking the potential of a novel generation of lithium niobate photodetectors, suited for harsh environments and for high levels of sensing platform integration.

2. Experimental setup for H_2 detection

The schematic of the experimental setup employed for hydrogen detection is shown in Fig. 1. The presented configuration allows i) non-contact measurements, since the detector and the gas are in two separate chambers, ii) two different pressure conditions for the gas flowing in the MPC and for the piezoelectric tuning forks, iii) easy comparison among different detectors.

The H_2 absorption feature at 4712.90 cm^{-1} [19] was targeted by a Nanoplus laser source, having a central emission wavelength of $\lambda = 2121.8$ nm and a maximum optical power of 21 mW. A Thorlabs Herriot MPC HC10L/M-M02 multi-pass cell (MPC) was selected to obtain a 10.4 m interaction pathlength between light and hydrogen molecules and partially compensate for the weakness of H_2 quadrupole transitions. As suggested by the manufacturer [37], a 500 mm focal length bi-convex lens prior to the MPC (L1 in Fig. 1) was employed and placed close to the collimating lens of the laser and at 500 mm from the center of the cell. This ensures that a collimated beam at the cell input does not lead to an overspill of light on the mirrors, causing background signals. Due to the multiple reflection and the losses on the mirror [37], a maximum optical power of 10 mW was measured at the MPC output and it was focused on the detector with a lens having a focal length of 50 mm (L2 in Fig. 1). The laser beam after L2 was acquired with a Spiricon Pyrocam IIIHR and the $1/e^2$ width of the intensity distribution

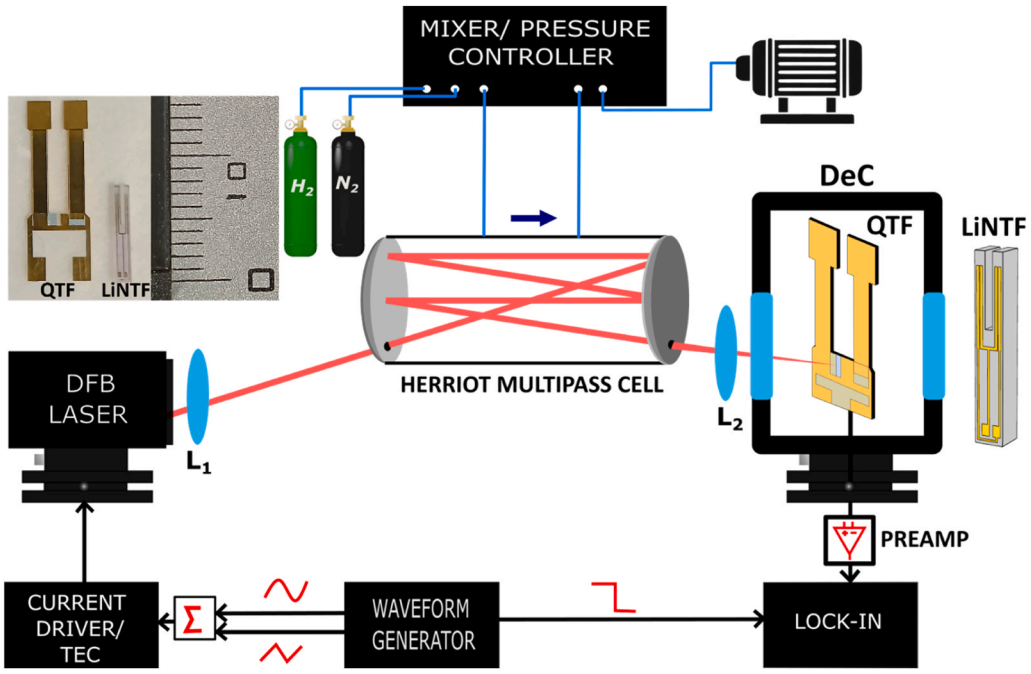

Fig. 1. Schematic of the experimental setup. DFB Laser – Distributed Feedback Laser, TEC – ThermoElectric Cooler, QTF- Quartz Tuning Fork, DeC – Detector Chamber. Inset: LiNTF- Lithium Niobate Tuning Fork (not in scale). On the left a picture showing the QTF and LiNTF is reported. A ruler is included to compare the dimensions of both tuning forks, with dimensions in millimeters.

was employed to compare the beam dimension with respect to the active area of the detectors [38–40]. Considering a gaussian fit for the intensity distribution and defining the beam diameter as twice the $1/e^2$ half width, a diameter of 0.328 ± 0.002 mm was measured in the focal point. In this experiment a QTF, as depicted in Fig. 1, and a LiNTF (shown in the inset of Fig. 1) were employed as photodetectors for H_2 sensing. A picture of both tuning forks is also shown, and their geometrical parameters are reported in Table 1. The tuning forks were placed in turn in a detection chamber (DeC), a stainless-steel vacuum-tight cell equipped with two wedged BaF_2 windows (Thorlabs WW01050-E1, AR Coating: 2–5 μm) with external dimensions 5x5x5 cm^3 [23]. A transimpedance amplifier was employed to convert the piezoelectric current generated by the tuning forks into an electric signal. An MCQ-INSTRUMENTS GM VACUUM 1.3 allowed both the stabilization of the pressure inside the MPC, together with a KNF vacuum pump, and the generation of several H_2:N_2 mixtures, diluting a pure hydrogen cylinder with a pure nitrogen cylinder for the calibration of the sensor. The purity of the H_2 and N_2 cylinders was grade 4.5, corresponding to a composition of 99.995 % pure gas. Therefore, the error on the concentration of each generated mixture is assumed to be determined by the uncertainty of the gas blender (MCQ Instruments GM VACUUM 1.3), as specified by the manufacturer. A pressure of 760 Torr in the MPC and a flow rate of 100 sccm were employed for the comparison reported in this work. The measurements were performed at ambient temperature (T = 23°). A Tektronix AFG 31000 waveform generator was employed to pursue a wavelength modulation (WM) detection scheme and provide a modulation signal (at a frequency that is half of the tuning forks resonance frequency) to the ITC4002QCL laser driver and the reference signal to the Zurich Instrument MFLI lock-in amplifier for the 2 f WM-detection of the tuning fork signal [41,42].

Table 1
Geometrical parameters of the lithium niobate tuning fork (LiNTF) and quartz tuning fork (QTF) employed in this work: L (prong length), T (thickness of the prong), w (thickness of the crystal) and s (spacing between prongs).

	L (mm)	T (mm)	w (mm)	s (mm)
QTF	Base: 7 Head: 2.4	Base: 1.4 Head: 2	0.25	1
LiNTF	3.18	0.45	1.25	0.35

3. Results and discussion

3.1. H_2 spectral characterization

Being H_2 a homonuclear molecule, its infrared absorption spectrum is limited to vibrational bands of low intensity due to quadrupole transitions. HITRAN Application Programming Interface (HAPI) [19] was

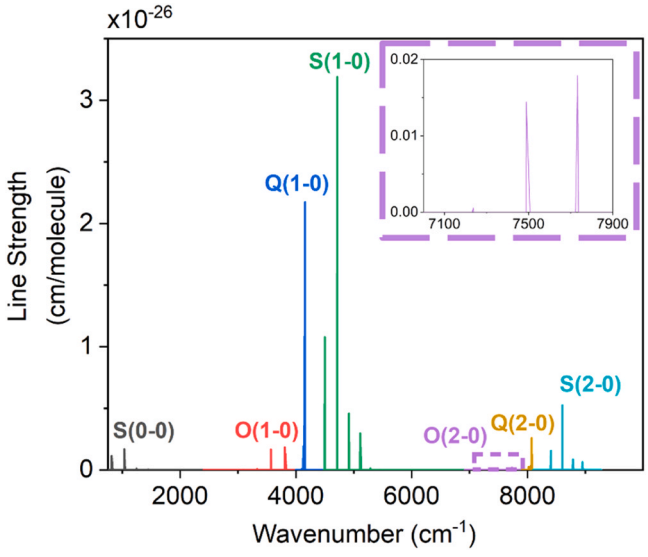

Fig. 2. H_2 spectral lines grouped according to the vibrational and angular momentum quantum states associated to each transition. (1−0) and (2−0) refer to the fundamental and vibrational band, respectively; O, Q, S correspond to the angular momentum quantum number ΔJ = -2, 0, 2, respectively. In the inset, a zoomed-in view on the absorption lines in the 7100–7900 cm^{-1} range is shown.

employed to simulate H_2 absorption spectrum, as depicted in Fig. 2.

H_2 absorption transitions can be grouped into two vibrational bands, fundamental (1−0) and overtone (2−0), which form O, Q and S branches corresponding to a variation of the angular momentum quantum number ΔJ = -2, 0, 2, respectively. As a result of the high values of the rotational constant (B ≈ 61 cm^{-1}) [43], the spectrum is extremely sparse and only a few absorption lines are observable for each vibrational band. The most intense H_2 quadrupole transition from the S (1−0) branch, located at 4712.90 cm^{-1} and with a linestrength of $3.18{\cdot}10^{-26}$ cm/molecule, was chosen to attain a reasonable detection limit compatible with most of the applications involving hydrogen generation and monitoring. Despite not being free from interference with the primary absorber gases, i.e. CH_4, H_2O, and CO_2, cross correlation is substantially weaker compared to other H_2 lines [11,19].

Before evaluating the LITES-based sensor performance, the spectral properties of the selected transition were investigated analyzing the detected 2f signal as a function of the pressure inside the MPC, which was acquired by means of a commercial photodetector (DET05D2 [44]) temporally used in place of the piezoelectric tuning forks for these preliminary tests. It is worth noticing that the outcome of this investigation is independent from the employed detector.

Firstly, the 2 f spectra of pure H_2 were acquired at four representative pressures within the MPC. The modulation depth (Δν), i.e. the amplitude of the sine wave modulation was optimized for each pressure and the normalized acquired signals are reported in Fig. 3.

As shown in the figure, the normalized acquired signals increase as a function of pressure, in the 300–900 Torr investigated range. The red and blue curves in Fig. 3 highlight the presence of a fringe pattern superimposed to the 2f signal. This distortion is more visible for the spectra with low SNRs and, as stated by the manufacturer [44], it is due to the comparable dimensions of the laser beam and the diameter of the active area of the detector (0.5 mm). Lambert beer law provides the dependence on pressure (P) of the detector signal, which in the limit of low absorption is given by [45]:

$$S(\nu,P) = k \bullet I(\nu) \bullet (1 - \alpha(\nu,P) \bullet L) = k \bullet I(\nu) \bullet (1 - N(P) \bullet \sigma(\nu,P) \bullet L), \quad (1)$$

where k is the conversion factor relating the detector signal to I(ν), the power impinging upon its sensitive area, L is the optical path and α(ν) is the absorption coefficient, expressed as the product between the molecule number density N(P) and the absorption cross section σ(ν,P). For an isolated spectral line, it results that σ(ν,P)=LS·Γ(ν,P), being LS the transition linestrength and Γ(ν,P) the line shape function. Thereby, the detector signal depends on the pressure via two factors: i) the number density, which increases with pressure, and ii) the absorption cross section, whose pressure dependency is related to the specific line shape function associated with the selected transition. Although the line shape function of most of the molecules is given by a Voigt function, multiple studies have shown that the Hartmann-Tran line profile best represents the line shape of H_2 quadrupole transitions by accounting for non-Voigt phenomena, such as speed dependency of collisional broadening and Dicke narrowing [11,46]. For small modulation depth, the in-phase component of the 2 f signal is proportional to the second derivative of Γ(ν,P) and it is maximized when the ratio between Δν and the half width at half maximum of the line shape function (HWHM) is equal to 2.2 [11]. The Δν values, employed to acquire the signals in Fig. 3 were used to calculate the HWHM at the different investigated pressures. HAPI was subsequently used to simulate the absorption cross section of H_2 S(1−0) transition employing both the Voigt and the Hartmann Tran (HT) functions as line shapes and the simulated absorption features are shown in Fig. 4a.

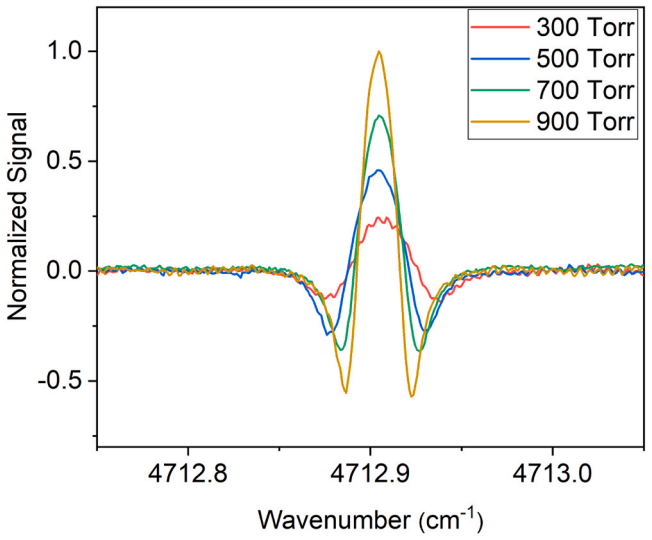

Fig. 3. 2 f spectra of 100 % H_2 acquired at 300, 500, 700, 900 Torr.

The absorption coefficient can be estimated from the Voigt and HT simulations of absorption cross section (see Eq. 1). In the Voigt simulations, the peak of the absorption cross section reduces by 6.7 % as the pressure increases from 300 Torr to 900 Torr. The numerical density increases with pressure, resulting in a peak absorption coefficient three times higher at 300 Torr than at 900 Torr. While in the same pressure range, the HT simulations yield a 38.4 % increase in hydrogen peak cross section. This corresponds to a fourfold increase in the absorption coefficient when the pressure is changed from 300 Torr to 900 Torr, which matches the increase observed in the signals shown in Fig. 3.

Furthermore, the broadening of the line shape functions was evaluated considering the HWHM of both the Voigt and HT simulations and compared in Fig. 4b with the Δν employed. The HWHMs of the Voigt simulations are higher compared to HT profile and slightly increase from 300 Torr to 900 Torr (5 %). In the same pressure range, the HWHMs of the HT profile decrease with pressure (56 %), as experimentally found and with an average relative error of 14 % on the employed Δν. This decreasing trend in the spectral width is attributed to the Dicke narrowing effect, which occurs when molecules undergo numerous collisions during absorption. This phenomenon induces a reduction of the mean velocity of the molecules, resulting in a narrowing of the Doppler width (0.0211 cm^{-1}) [47–49]. Dicke narrowing, usually masked by other broadening mechanisms for other molecules, mainly determines the H_2 line shape up to 1500 Torr due to the high frequency of velocity changing collisions (0.0481 $cm^{-1}atm^{-1}$) and the H_2 low collisional broadening (0.0019 $cm^{-1}atm^{-1}$) [19,46]. Only at higher pressures, not accessible with the employed setup, speed-dependent collisional broadening emerges causing an increase of spectral width [19]. HT line shape takes into account both speed dependent broadening and narrowing of Doppler width, resulting in an H_2 absorption coefficient at atmospheric pressure twice as high as that erroneously predicted by the Voigt line shape. Despite the observed higher signal at 900 Torr, the MPC was operated at the atmospheric pressure for hydrogen sensing because it is more suitable for real word applications.

3.2. QTF-based LITES sensor

The QTF employed as photodetector was a custom T-shaped tuning fork with carved groove on the surface of the prongs, which already demonstrated the best performance in LITES detection (QTF #2 in [24]). The QTF was enclosed in vacuum tight detector chamber (DeC in Fig. 1), and it was operated at atmospheric pressure (760 Torr). The green rectangle in Fig. 5a defines the portion of the QTF available to employ the resonator as photodetector for H_2 detection.

The LITES signal was optimized focusing the laser beam on the position highlighted by the red circle in Fig. 5a, as it is close to the maximum strain region of the QTF [22]. From the analysis of the layers composing the QTF in the focusing point (Fig. 5b), it results that the

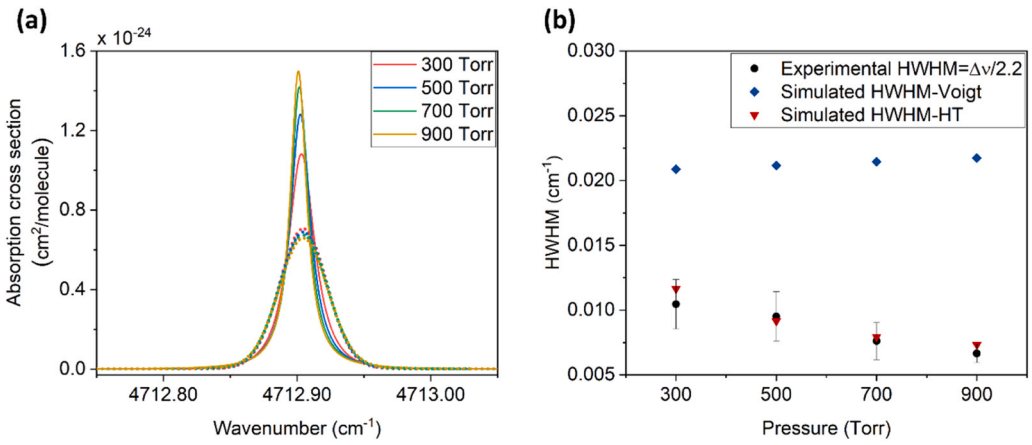

Fig. 4. a) Simulated absorption cross section of H_2 at 300, 500, 700, 900 Torr employing the Voigt line shape (dashed line) and the Hartman-Tran line shape (solid line). b) Simulated and experimental HWHM as function of pressure. Experimental HWHM was calculated as HWHM = $\Delta\nu/2.2$, being $\Delta\nu$ the optimal modulation depth determined experimentally for each pressure.

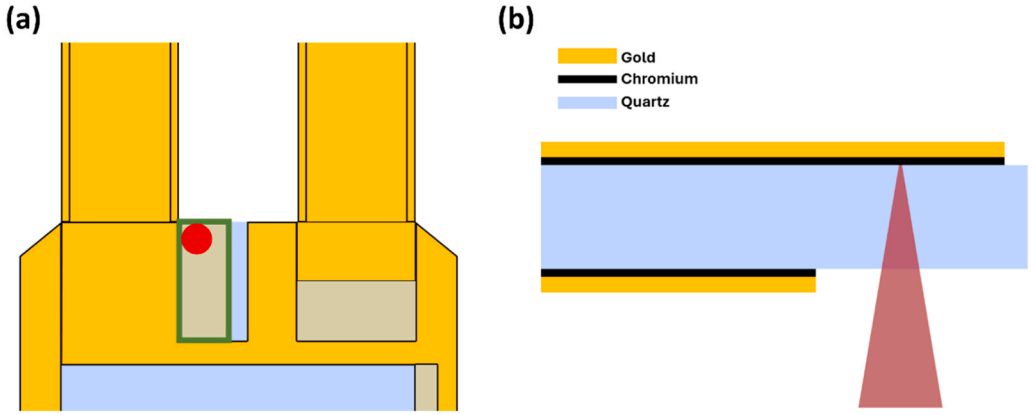

Fig. 5. a) Detail of the QTF portion where the laser beam is focused. The green rectangle highlights the actual active area for the detection of H_2 and the red circle represents the laser beam. b) Sketch of the layers composing the QTF zone where the beam is aligned. The red triangle represents the laser beam.

radiation passes through the 250 μm-thick quartz layer without a significant attenuation (the transmittivity is greater than 90 % at wavelengths close to 2 μm [22]) and it is completely absorbed in the 50 Å-thick chromium layer, having an absorption coefficient as high as $3.97{\cdot}10^5$ cm^{-1} at the laser central wavelength [50]. Therefore, the active area actually available for focusing the laser beam upon the front surface is basically delimited by the gold contacts and it is slightly smaller than $0.7{\times}1.0$ mm^2, as highlighted with the green rectangle in Fig. 5a. The normalized electrical characterization of the employed resonator is reported in Fig. 6.

At atmospheric pressure, the Lorentzian fit of the measured data (R^2>0.99) returned a fundamental resonance frequency (f_0) of 9763.57 Hz and a quality factor Q of 11400. The extracted f_0 was employed to acquire the 2f spectra of H_2 shown in Fig. 7a, focusing the beam on the maximum strain point of the QTF [22].

The peak values of the signals in Fig. 7a are plotted as a function of the corresponding H_2 concentration in Fig. 7b to obtain the calibration curve for the QTF operated at atmospheric pressure. The best linear fit (R^2>0.999) of the measured data returned a slope of $6.59{\cdot}10^{-5}$ V/% and an intercept of $-2.90{\cdot}10^{-4}$ V.

The noise level was evaluated as the standard deviation of the signal acquired in the tuning range shown in Fig. 7a, while pure nitrogen was in the MPC. Considering a noise level of $3.47{\cdot}10^{-5}$ V, a 1-σ MDL of 0.50 % was achieved at 0.1 s of integration time.

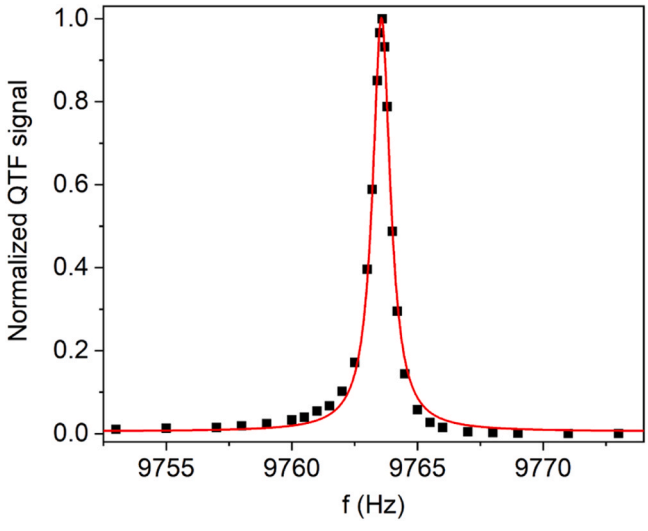

Fig. 6. Normalized electrical characterization of the QTF at 760 Torr. Black squares represent the measured data, while the red curve represents the best Lorentzian fit superimposed to the data.

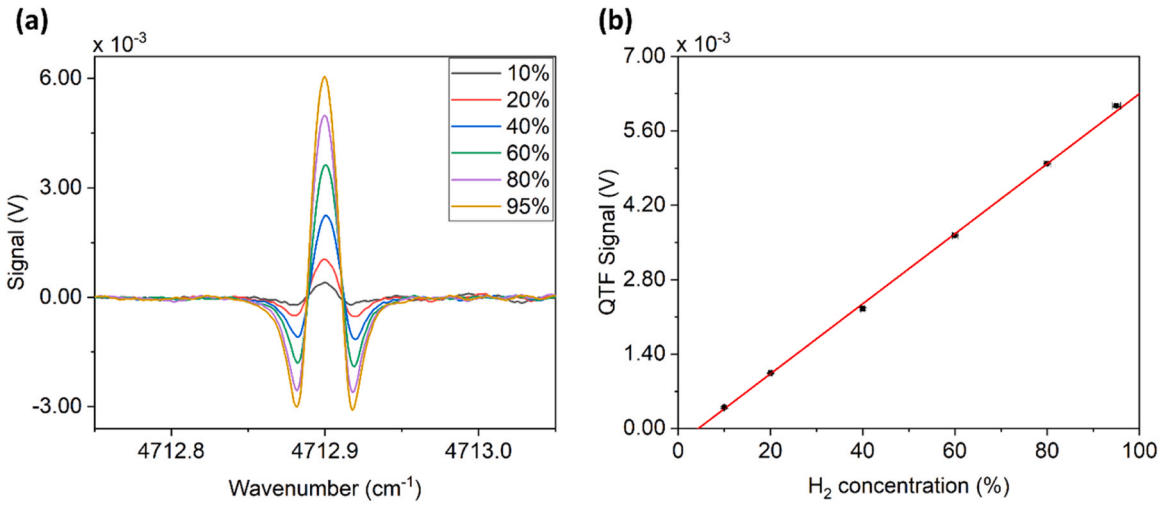

Fig. 7. a) 2-f spectra of hydrogen in the 0–100 % concentration range, acquired with the QTF at atmospheric pressure. b) Calibration curve of the H_2 2f spectra peak (black squares) and the best linear fit (red curve) is superimposed to the experimental data.

3.3. LiNTF-based LITES sensor

The QTF in Fig. 1 was replaced by a LiNTF and it was operated at 760 Torr to compare the two piezoelectric resonators as infrared detectors for H_2 detection. The layer composition of the resonator is shown in Fig. 8.

The front surface of the LiNTF, shown in the inset of Fig. 1, is characterized by the presence of the gold electrodes, employed to collect the electric charges generated via the piezoelectric effect and a chromium layer, used to adhere the gold electrodes to the LiNTF. Since the back surface of the LiNTF does not present any other material but lithium niobate [33], the laser beam was focused there (as shown in Fig. 8). Due to the low absorption at the laser wavelength (the transparency window of lithium niobate ranges from 350 nm up to 4.5 μm [51]) the radiation passes through the whole 1.25 mm thickness of the resonator substantially unabsorbed, reaching the chromium layer. As in the QTF-based sensor, the strong absorption coefficient of chromium allows exploiting the piezoelectric effect to convert the absorbed radiation into an electric signal [22], dominating the weak pyroelectric effect occurring in lithium niobate [52,53]. The position of the laser beam upon the LiNTF surface was varied to explore the region of maximum strain and optimize the LITES signal. For this optimization, the MPC was filled with 100 % of H_2 and the LiNTF position was varied with a translation stage. The homogeneity of the back surface allowed a complete scan, both along the length of the prong (vertical scan), and along the width of the resonator (horizontal scan). As it was verified for the QTF, the vertical scan investigation confirmed that the laser beam focus point optimizing the LITES signal is found at the base of the 3.18 mm-long prong, where the strain field is maximum [22]'[33]. At this vertical position, highlighted by the green rectangle in Fig. 9a, a horizontal scan was performed, with a normalized trend of the LITES signal shown in Fig. 9b.

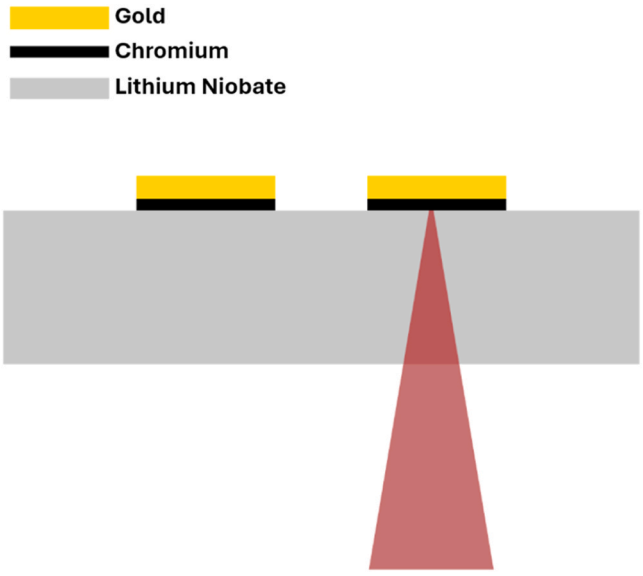

Fig. 8. Sketch of the layers composing the LiNTF. The red triangle represents the laser beam.

The four peaks of the LITES signal in the horizontal scan correspond to positions of the laser beam spot aligned with the centers of the electrodes. A peak decrease of ~19 % was measured between electrodes A and D, which is well above the relative error on the peak signal (~1.5 %). While this variation is partly due to the finite resolution of the translation stage, it was consistently observed and confirmed through repeated measurements. The peak differences can be attributed to the ratio between the laser beam diameter and the width of the gold electrodes (~0.2 mm [33]), which may slightly vary among electrodes. Additionally, inhomogeneities in the deposition of the chromium adhesion layer, used to bind the gold electrodes to the lithium niobate surface, may contribute to the signal variation.

Considering the measured signal, the beam was focused on the electrode D for the following measurements. Due to the high parasitic capacitance [31,54], the resonance properties of the employed LiNTF can be better measured through an optical characterization, shown in Fig. 10: the MPC was filled with 100 % of H_2 and the peak of the 2f signal was acquired as a function of the frequency of the laser modulating signal.

From the analysis of the experimental data, the Lorentzian fit returned an f_0 of 40627.61 Hz and a Q of 3100. The retrieved modulation frequency was provided to the laser to acquire the 2f spectra corresponding to different hydrogen concentrations, as shown in Fig. 11a.

From the experimental data shown in Fig. 11b, the linear fit (R^2>0.99) returned a slope of $1.34{\cdot}10^{-5}$V/% and an offset of $-4.96{\cdot}10^{-7}$V and, considering a noise level of $2.00{\cdot}10^{-5}$V, an MDL of 1.50 % was achieved at 0.1 s of integration time with the LiNTF. Considering the calculated values, the difference in the MDLs could mainly rely on the quality factor values of the two resonators.

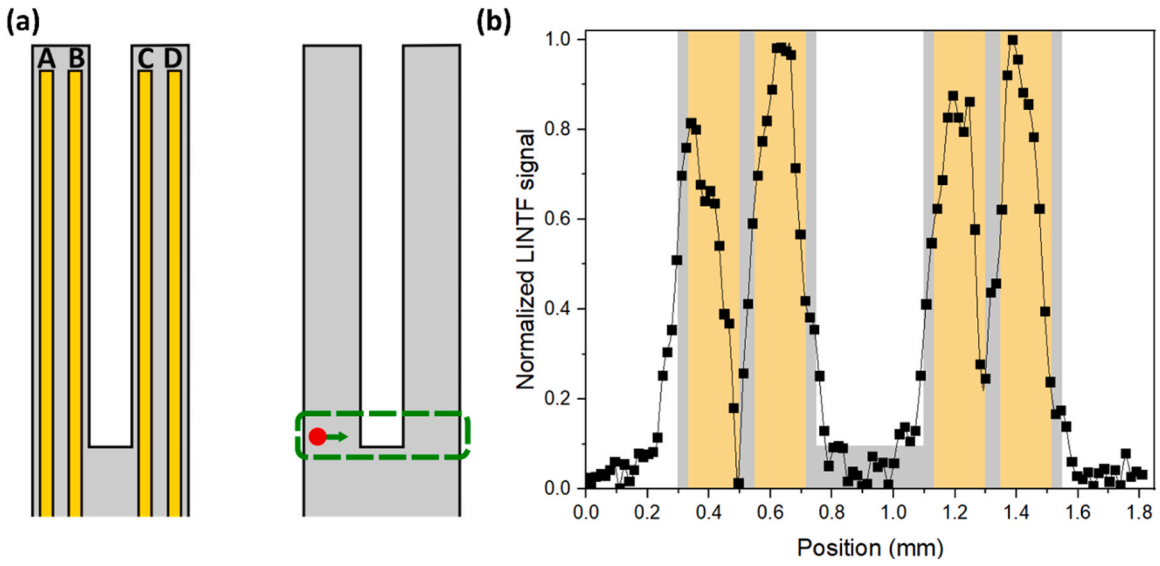

Fig. 9. a) Front (left) and back (right) surface of the LiNTF employed as photodetector. The position of the beam, represented by a red circle, was varied in the zone highlighted by the green rectangle for the horizontal scan. The electrodes (A-D) are employed to collect the electric charges generated via the piezoelectric effect. b) Normalized LITES signal as a function of the horizontal focusing point. The signal is optimized when the laser beam is focused on the electrode D.

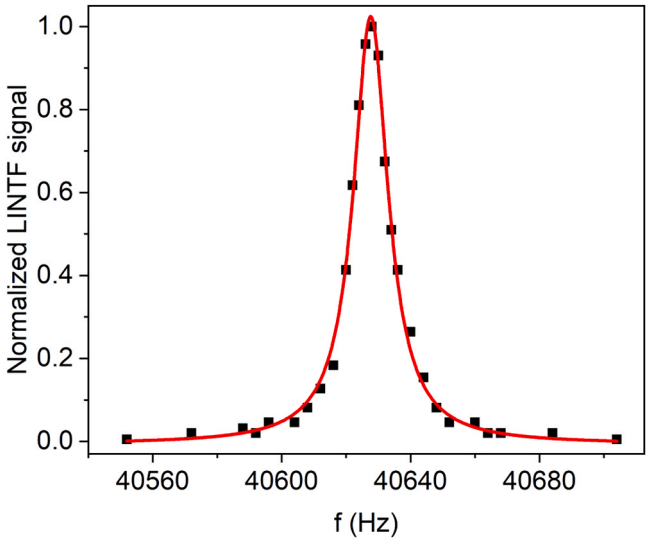

Fig. 10. Normalized optical characterization of the LiNTF at 760 Torr. Black squares represent the measured data, while the red curve represents the best Lorentzian fit superimposed to the data.

3.4. Stability analysis for the QTF- and the LiNTF-based sensors

The Allan-Werle deviation analysis was employed to assess the stability for the H_2 detection with the two selected piezoelectric detectors [55]. This comparison was carried out with both tuning forks at atmospheric pressure, with a constant flow of pure nitrogen in the MPC and at an integration time of 0.1 s. The 2f signal was acquired with the laser wavelength locked on the H_2 absorption line and was then converted into MDL using the calibration slopes previously determined, as shown in Fig. 12.

For the H_2 detection with a QTF, the Allan-Werle Deviation (ADEV) analysis (Fig. 12a) highlights a high bias instability [56–58] since the minimum of the deviation occurs at an integration time as small as 2 s. ADEV analysis for the QTF was performed several times, verifying the optimum alignment conditions and confirming the instability issues. As already commented for the photodetector, an active area of the QTF comparable with the dimensions of the beam diameter can give rise to signal distortions and, in addition for the QTF, the gold electrodes on the resonator surface could generate undesired reflections of the incident light, which could determine in turn possible interferences altering the stability of the signal. A sensitive improvement could only be obtained through a massive modification of the optics downhill the cell to pursue a suitable beam shaping. Conversely, the ADEV analysis of the LiNTF returned the trend expected for a sensing system mostly limited by white noise. Indeed, the deviation decreases from 0.1 s to 64 s of integration time, and thus this means that the H_2 MDL can be decreased at longer integration time. Specifically, the MDL improves to 0.1 % at 64 s, a 17-fold reduction compared to the 0.1 s measurement (Fig. 12b). Although the active area of the LiNTF is smaller than the QTF one (see the resonator dimensions in [33]), the uniformity of the surface where the laser beam is focused provide a higher long-term stability in H_2 detection.

From a comparison of the detection limits, it can be noticed that the 9.8 kHz QTF reported in this work demonstrated an MDL of 0.5 % at an integration time of 0.1 s, which is comparable with the 0.3 % MDL obtained by Yufei Ma et al. in [29] using the 30 kHz QTF, without denoising algorithms. The slightly better result stems from a longer 0.7 s integration time during the spectral scans.

Compared to these two QTFs, the LiNTF initially shows a worse MDL (1.5 % at 0.1 s), primarily due to its lower quality factor (Q=3100). Nevertheless, its mechanical stability and structural usability thanks to the large focusing area provides a significant noise reduction at longer integration times, enabling a sensitivity improvement down to 0.1 % at 64 s.

As an additional proof of the long-term stability of the LiNTF-based LITES sensor, the LiNTF signal was acquired at an integration time of 0.1 s over a 24-hour period while flowing a mixture of 10 % H_2 diluted in N_2 through the MPC. The recorded signal was subsequently converted into concentration values using the calibration curve shown in Fig. 11 and the obtained results are shown in Fig. 13.

The measured data yielded an average concentration of $\mu = 10.4$ %, which agrees with the expected concentration of the generated mixture within the observed 1σ standard deviation of 1.5 %. Furthermore, these fluctuations are also consistent with the MDL previously determined for the LiNTF-based LITES sensor. These results provide further evidence of both the accuracy and the long-term stability of the sensor, demonstrating its capability for continuous real-time H_2 monitoring.

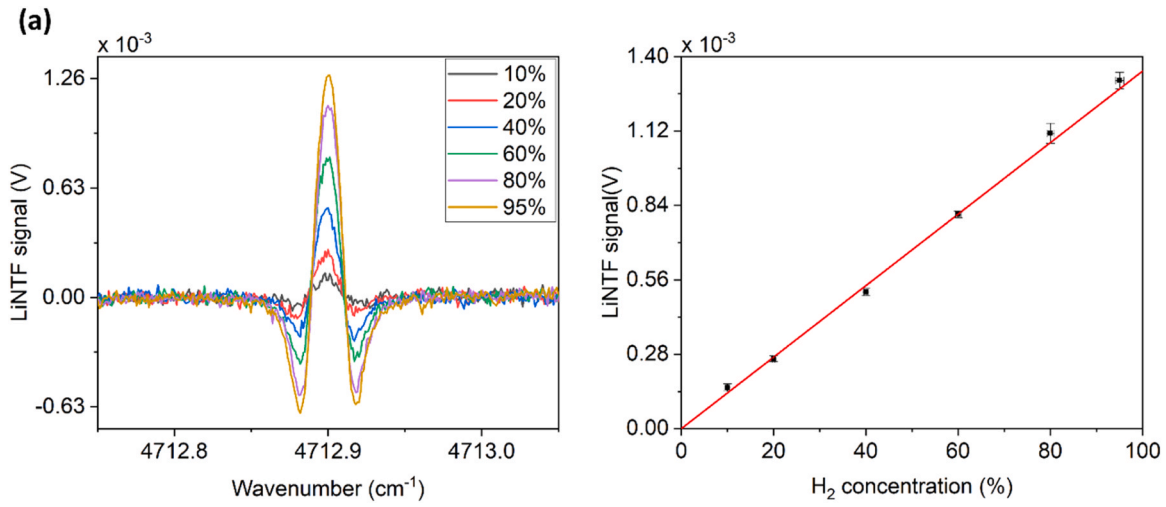

Fig. 11. a) 2-f spectra of hydrogen in the 0–100 % concentration range, acquired with the LiNTF at atmospheric pressure. b) Calibration curve of the H_2 2f spectra peak (black squares) and the best linear fit (red curve) is superimposed to the experimental data.

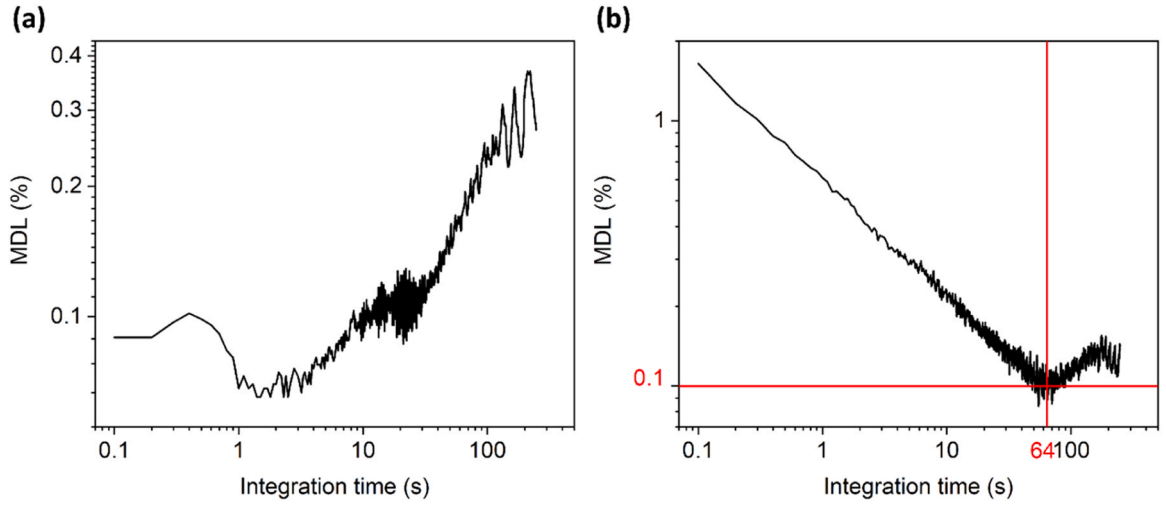

Fig. 12. Allan-Werle deviation analysis for a) the QTF- and b) the LiNTF-based LITES sensors.

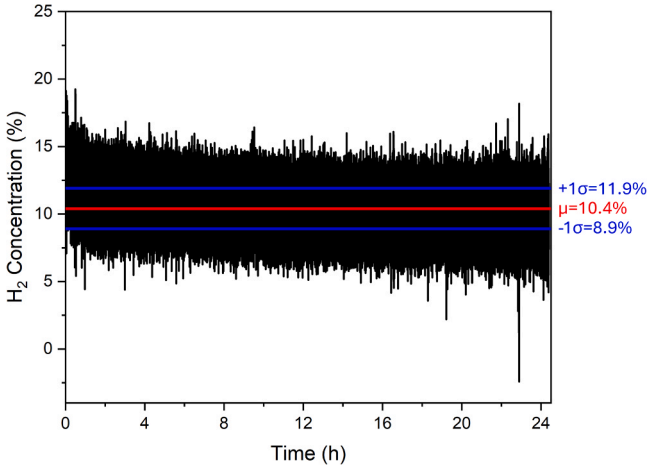

Fig. 13. H_2 concentration measured over a 24-hour period with the LiNTF-based LITES sensor while flowing a 10 % H_2 in N_2 mixture through the MPC. The integration time was set to 0.1 ms. The red line indicates the mean value (μ = 10.4 %), while the blue lines represent the ±1σ range, where σ is the standard deviation, corresponding to 11.9 % and 8.9 %.

4. Conclusions

In this work, we presented a detailed study on the spectral properties of molecular hydrogen together with a comparison between two piezoelectric tuning forks, composed of quartz and lithium niobate, respectively, for hydrogen detection in a Light-Induced Thermoelastic Spectroscopy (LITES) configuration. From the study of the selected hydrogen quadrupole transition, it resulted that the HWHM of the 2 f signal reduces with an increase of the pressure, because of the Dicke effect, and that the peak of the signal increases at higher pressures. This experimental evidence determined an operating pressure of 700 Torr. The two resonators were employed as infrared detectors in a TDLAS experimental setup, implementing a MPC for the detection of the weak H_2 absorption feature at 2121.8 nm. Since both quartz and lithium niobate do not exhibit strong absorption coefficients within the laser tuning range, the chromium layer promoting the adhesion of the gold electrodes upon the tuning fork surfaces allows the conversion of optical power into an electric signal through piezoelectric effect. The H_2 detection with the QTF was carried out operating the resonator at atmospheric pressure and a detection limit of 0.50 % at 0.1 s of integration time was achieved. Replacing the QTF with a LiNTF in the same experimental setup, an MDL of 1.50 % was demonstrated at 0.1 s of

integration time. The difference of the MDLs mainly depends on the quality factor of the resonators. Finally, the stability in the H_2 detection was investigated for both piezoelectric detectors. The Allan-Werle analysis returned a long-term instability for the QTF in this setup, that could be addressed to the dimension of the focusing window upon the QTF and to the back reflections from the gold contact. The employed LiNTF is characterized by much smaller overall dimensions, but the absence of gold contacts deposited on the focusing side of the LiNTF makes the alignment more stable and avoids the interaction of the light beam with edges and reflecting surfaces. In this case, the LiNTF demonstrated stability for the hydrogen detection up to 64 s of integration time, corresponding to an MDL of 0.1 %. The detection performance of these detectors can be improved either engineering the gold electrodes layout in QTFs to provide a uniform surface for the alignment of the laser beam or varying the geometry of the LiNTF to improve the SNR in the H_2 detection. In future, absorbing layers can be applied on the tuning forks' surface and dopants added during the manufacturing process to enhance the absorbance of the LiNTF and further improve the performances as light detectors. Finally, unlike quartz, lithium niobate enables the integration of optical and acoustic components on a single chip, thus making lithium-niobate-on-insulator a highly suitable platform for the next-generation of compact and integrated sensing systems.

CRediT authorship contribution statement

Mariagrazia Olivieri: Writing – original draft, Software, Investigation, Formal analysis, Data curation. **Giansergio Menduni**: Writing – original draft, Visualization, Validation, Supervision, Methodology, Investigation, Conceptualization. **Andrea Zifarelli:** Writing – review & editing, Visualization, Supervision, Formal analysis. **Aldo F.P. Cantatore**: Writing – review & editing, Visualization, Formal analysis. **Marilena Giglio:** Writing – review & editing, Visualization, Supervision, Formal analysis. **Huseyin R. Seren:** Writing – review & editing, Visualization, Supervision, Resources, Project administration. **Miguel Gonzalez**: Writing – review & editing, Visualization, Supervision, Resources, Project administration, Conceptualization. **Huadan Zheng**: Writing – review & editing, Visualization, Supervision, Formal analysis. **Hongpeng Wu**: Writing – review & editing, Visualization, Supervision, Formal analysis. **Lei Dong**: Writing – review & editing, Visualization, Supervision, Formal analysis. **Pan Luo**: Writing – review & editing, Visualization, Supervision, Resources, Project administration. **Pietro Patimisco**: Writing – review & editing, Visualization, Supervision, Funding acquisition, Formal analysis. **Vincenzo Spagnolo**: Writing – review & editing, Visualization, Supervision, Funding acquisition, Formal analysis. **Angelo Sampaolo**: Writing – review & editing, Visualization, Supervision, Funding acquisition, Formal analysis, Conceptualization.

Declaration of Competing Interest

The authors declare that they have no known competing financial interests or personal relationships that could have appeared to influence the work reported in this paper.

Acknowledgements

The authors from Dipartimento Interateneo di Fisica di Bari acknowledge financial support from PNRR MUR project PE0000021-NEST - Network 4 Energy Sustainable Transition, from PNRR MUR project PE0000023-NQSTI, and project MUR – Dipartimenti di Eccellenza 2023–2027 – Quantum Sensing and Modelling for One-Health (QuaSiModO). We thank Prof. Donato Creanza (Dipartimento Interateneo di Fisica M. Merlin, Università degli Studi di Bari Aldo Moro e Politecnico di Bari) for helping us in bonding and wiring of the lithium niobate tuning fork.

Data availability

Data will be made available on request.

References

[1] W.J. Buttner, M.B. Post, R. Burgess, C. Rivkin, An overview of hydrogen safety sensors and requirements, Int. J. Hydrog. Energy 36 (2011) 2462–2470, https://doi.org/10.1016/j.ijhydene.2010.04.176.
[2] T. Hübert, L. Boon-Brett, G. Black, U. Banach, Hydrogen sensors – a review, Sens. Actuators B Chem. 157 (2011) 329–352, https://doi.org/10.1016/J.SNB.2011.04.070.
[3] T. Sahoo, P. Kale, T. Sahoo, P. Kale, Work Function-Based Metal–Oxide–Semiconductor hydrogen sensor and its functionality: a review, Adv. Mater. Interfaces 8 (2021), https://doi.org/10.1002/admi.202100649.
[4] M. Lackner, Tunable diode laser absorption spectroscopy (TDLAS) in the process industries - a review, Rev. Chem. Eng. 23 (2007) 65–147, https://doi.org/10.1515/REVCE.2007.23.2.65.
[5] J. Sun, J. Chang, C. Wang, J. Shao, Tunable diode laser absorption spectroscopy for detection of multi-component gas: a review, Appl. Spectrosc. Rev. (2024), https://doi.org/10.1080/05704928.2024.2302608.
[6] A. Annunziato, F. Anelli, P. Le Pays, D.U. Teilleul, S. Cozic, S. Poulain, F. Prudenzano, Fused optical fiber combiner based on indium fluoride glass: perspectives for mid-IR applications, Opt. Express 30 (24) (2022) 44160–44174, https://doi.org/10.1364/OE.471090.
[7] M.A. Bolshov, Y.A. Kuritsyn, Y.V. Romanovskii, Tunable diode laser spectroscopy as a technique for combustion diagnostics, Spectrochim. Acta Part B At. Spectrosc. 106 (2015) 45–66, https://doi.org/10.1016/J.SAB.2015.01.010.
[8] X.L. Yu, F. Li, L.H. Chen, X.Y. Chang, A tunable diode-laser absorption spectroscopy (TDLAS) thermometry for combustion diagnostics, 15th, AIAA Int. Sp. Planes Hypersonic Syst. Technol. Conf. (2008), https://doi.org/10.2514/6.2008-2657.
[9] S. Reuter, J.Santos Sousa, G.Daniel Stancu, al -, J. Röpcke, G. Lombardi, A. Rousseau, P.B. Davies, Application of mid-infrared tuneable diode laser absorption spectroscopy to plasma diagnostics: a review, Plasma Sources Sci. Technol. 15 (2006) S148, https://doi.org/10.1088/0963-0252/15/4/S02.
[10] A. Sepman, J. Wennebro, J. Fernberg, H. Wiinikka, Following fuel conversion during biomass gasification using tunable diode laser absorption spectroscopy diagnostics, Fuel 374 (2024) 132374, https://doi.org/10.1016/j.fuel.2024.132374.
[11] V. Avetisov, O. Bjoroey, J. Wang, P. Geiser, K.G. Paulsen, Hydrogen sensor based on tunable diode laser absorption spectroscopy, Sensors 19 (2019), https://doi.org/10.3390/s19235313.
[12] S. Kassi, A. Campargue, Electric quadrupole transitions and collision-induced absorption in the region of the first overtone band of H2 near 1.25 μm, J. Mol. Spectrosc. 300 (2014) 55–59, https://doi.org/10.1016/J.JMS.2014.03.022.
[13] A. Campargue, S. Kassi, K. Pachucki, J. Komasa, The absorption spectrum of H2: CRDS measurements of the (2-0) band, review of the literature data and accurate ab initio line list up to 35 000 cm−1, Phys. Chem. Chem. Phys. 14 (2011) 802–815, https://doi.org/10.1039/C1CP22912E.
[14] Y. Shi, Z. Hu, M. Niu, T. Li, H. Li, H. Liu, X. Li, High-sensitive double incidence multi-pass cell for trace gas detection based on TDLAS, Sens. Actuators B Chem. 412 (2024) 135829, https://doi.org/10.1016/J.SNB.2024.135829.
[15] R. Kong, J. Huang, P. Liu, X. Zhou, X. Zhou, Real-time breath gas analysis of methane using a multipass cell-based near-infrared gas sensor, Biomed. Opt. Express 15 (7) (2024) 4207–4219, https://doi.org/10.1364/BOE.528923.
[16] T. Yang, X. Wu, G. Guo, X. Guo, T. Gong, Y. Tian, X. Sun, X. Qiu, H. Yang, C. Fittshen, C. Li, A miniaturized multipass cell for measurement of O2 concentration in vials based on TDLAS, Opt. Lasers Eng. 163 (2023) 107454, https://doi.org/10.1016/j.optlaseng.2022.107454.
[17] L. Dong, F.K. Tittel, N.P. Sanchez, Y. Yu, A. Sampaolo, C. Li, H. Wu, C. Zheng, R. J. Griffin, Compact TDLAS based sensor design using interband cascade lasers for mid-IR trace gas sensing, Opt. Express 24 (6) (2016) A528–A535, https://doi.org/10.1364/OE.24.00A528.
[18] T. Liang, S. Qiao, X. Liu, Y. Ma, Highly sensitive hydrogen sensing based on tunable diode laser absorption spectroscopy with a 2.1 μm diode laser, Chemosens 2022 10 (2022) 321, https://doi.org/10.3390/CHEMOSENSORS10080321.
[19] R.V. Kochanov, I.E. Gordon, L.S. Rothman, P. Wcisło, C. Hill, J.S. Wilzewski, HITRAN application programming interface (HAPI): a comprehensive approach to working with spectroscopic data, J. Quant. Spectrosc. Radiat. Transf. 177 (2016) 15–30, https://doi.org/10.1016/J.JQSRT.2016.03.005.
[20] S. Cakmakyapan, P.K. Lu, A. Navabi, M. Jarrahi, Gold-patched graphene nanostripes for high-responsivity and ultrafast photodetection from the visible to infrared regime, Light Sci. Appl. 2018 7 (2018) 1–9, https://doi.org/10.1038/s41377-018-0020-2.
[21] C. Liu, J. Guo, L. Yu, J. Li, M. Zhang, H. Li, Y. Shi, D. Dai, Silicon/2D-material photodetectors: from near-infrared to mid-infrared, Light Sci. Appl. 2021 10 (2021) 1–21, https://doi.org/10.1038/s41377-021-00551-4.
[22] T. Wei, A. Zifarelli, S. Dello Russo, H. Wu, G. Menduni, P. Patimisco, A. Sampaolo, V. Spagnolo, L. Dong, High and flat spectral responsivity of quartz tuning fork used as infrared photodetector in tunable diode laser spectroscopy, Appl. Phys. Rev. 8 (2021), https://doi.org/10.1063/5.0062415.
[23] A. Zifarelli, A. Sampaolo, P. Patimisco, M. Giglio, M. Gonzalez, H. Wu, L. Dong, V. Spagnolo, Methane and ethane detection from natural gas level down to trace concentrations using a compact mid-IR LITES sensor based on univariate

calibration, Photoacoustics 29 (2023) 2213–5979, https://doi.org/10.1016/j.pacs.2023.100448.
[24] S.Dello Russo, A. Zifarelli, P. Patimisco, A. Sampaolo, T. Wei, H. Wu, L. Dong, V. Spagnolo, Light-induced thermo-elastic effect in quartz tuning forks exploited as a photodetector in gas absorption spectroscopy, Opt. Express 28 (2020), https://doi.org/10.1364/OE.393292.
[25] R. Wang, S. Qiao, Y. He, Y. Ma, Highly sensitive laser spectroscopy sensing based on a novel four-prong quartz tuning fork, OptoElectron. Adv. 0 (2025) 240275, https://doi.org/10.29026/OEA.2025.240275.
[26] X. Liu, S. Qiao, G. Han, J. Liang, Y. Ma, Highly sensitive HF detection based on absorption enhanced light-induced thermoelastic spectroscopy with a quartz tuning fork of receive and shallow neural network fitting, Photoacoustics 28 (2022) 100422, https://doi.org/10.1016/J.PACS.2022.100422.
[27] Y. Ma, Y. He, P. Patimisco, A. Sampaolo, S. Qiao, X. Yu, F.K. Tittel, V. Spagnolo, Ultra-high sensitive trace gas detection based on light-induced thermoelastic spectroscopy and a custom quartz tuning fork, Appl. Phys. Lett. 116 (2020) 1–4, https://doi.org/10.1063/1.5129014.
[28] F.K. Tittel, Y. Ma, X. Yu, Y. He, Y. Tong, Quartz-tuning-fork enhanced photothermal spectroscopy for ultra-high sensitive trace gas detection, Opt. Express 26 (24) (2018) 32103–32110, https://doi.org/10.1364/OE.26.032103.
[29] Y. Ma, T. Liang, S. Qiao, X. Liu, Z. Lang, Highly sensitive and fast hydrogen detection based on Light-Induced thermoelastic spectroscopy, Ultra Sci. 3 (2023) 1–9, https://doi.org/10.34133/ultrafastscience.0024.
[30] M. Tang, D. Chen, M. Zhang, F. Jiang, Y. Wang, Optimized design of lithium niobate tuning forks for the measurement of fluid characteristic parameters, Micromachines 2023 14 (2023) 2138, https://doi.org/10.3390/MI14122138.
[31] M. Gonzalez, H.R. Seren, G. Ham, E. Buzi, G. Bernero, M. Deffenbaugh, Viscosity and density measurements using mechanical oscillators in oil and gas applications, IEEE Trans. Instrum. Meas. 67 (2018) 804–810, https://doi.org/10.1109/TIM.2017.2761218.
[32] Y. Liu, R. Difoggio, K. Sanderlin, L. Perez, J. Zhao, Measurement of density and viscosity of dodecane and decane with a piezoelectric tuning fork over 298–448 K and 0.1–137.9 MPa, Sens. Actuators A Phys. 167 (2011) 347–353, https://doi.org/10.1016/j.sna.2011.03.017.
[33] A.F.P. Cantatore, G. Menduni, A. Zifarelli, P. Patimisco, M. Gonzalez, H.R. Seren, V. Spagnolo, A. Sampaolo, Lithium niobate - enhanced photoacoustic spectroscopy, Photoacoustics 35 (2023), https://doi.org/10.1016/J.PACS.2023.100577.
[34] M. Toda, M. Thompson, A. Sirven, C. Nordin, The influence of oil density and viscosity on the behavior of a lithium niobate tuning fork cantilever, IEEE Int. Ultrason. Symp. IUS (2012), https://doi.org/10.1109/ULTSYM.2012.0268.
[35] P. Patimisco, A. Sampaolo, L. Dong, M. Giglio, G. Scamarcio, F.K. Tittel, V. Spagnolo, Analysis of the electro-elastic properties of custom quartz tuning forks for optoacoustic gas sensing, Sens. Actuators B Chem. 227 (2016) 539–546, https://doi.org/10.1016/j.snb.2015.12.096.
[36] R.R. Xie, G.Q. Li, F. Chen, G.L. Long, Microresonators in lithium niobate thin films, Adv. Opt. Mater. 9 (2021) 2100539, https://doi.org/10.1002/ADOM.202100539.
[37] Herriott cells for multipass absorption spectroscopy, ⟨https://www.thorlabs.com/newgrouppage9.cfm?objectgroup_id=12671⟩.
[38] D.L. Shealy, J.A. Hoffnagle, Laser beam shaping profiles and propagation, Appl. Opt. 45 (2006) 5118–5131, https://doi.org/10.1364/AO.45.005118.
[39] J. Alda, Laser and Gaussian beam propagation and transformation, Encycl. Opt. Photon. Eng. Second Ed. (2015) 1193–1207, https://doi.org/10.1081/E-EOE2-120009751.
[40] F.M. Dickey, Laser beam shaping: Theory and Techniques, second ed., 2014, pp. 1–568, https://doi.org/10.1201/b17140.
[41] J. Wang, H. Wu, A. Sampaolo, P. Patimisco, V. Spagnolo, S. Jia, L. Dong, Quartz-enhanced multiheterodyne resonant photoacoustic spectroscopy, Light Sci. Appl. 2024 13 (2024) 1–10, https://doi.org/10.1038/s41377-024-01425-1.
[42] B. Li, G. Menduni, M. Giglio, P. Patimisco, A. Sampaolo, A. Zifarelli, H. Wu, T. Wei, V. Spagnolo, L. Dong, Quartz-enhanced photoacoustic spectroscopy (QEPAS) and beat Frequency-QEPAS techniques for air pollutants detection: a comparison in terms of sensitivity and acquisition time, Photoacoustics 31 (2023) 100479, https://doi.org/10.1016/J.PACS.2023.100479.
[43] C.C. Costain, Determination of molecular structures from ground state rotational constants, J. Chem. Phys. 29 (1958) 864–874, https://doi.org/10.1063/1.1744602.
[44] Thorlabs - DET05D2 InGaAs Detector, 900–2600 nm, 17 ns Rise Time, 0.2 mm2, Universal 8-32 / M4 Mounting Holes, ⟨https://www.thorlabs.com/thorproduct.cfm?partnumber=DET05D2#ad-image-0⟩.
[45] P. Kluczynski, J. Gustafsson, Å.M. Lindberg, O. Axner, Wavelength modulation absorption spectrometry - an extensive scrutiny of the generation of signals, Spectrochim. Acta Part B At. Spectrosc. 56 (2001) 1277–1354, https://doi.org/10.1016/S0584-8547(01)00248-8.
[46] P. Wcisło, I.E. Gordon, H. Tran, Y. Tan, S.M. Hu, A. Campargue, S. Kassi, D. Romanini, C. Hill, R.V. Kochanov, L.S. Rothman, The implementation of non-Voigt line profiles in the HITRAN database: H2 case study, J. Quant. Spectrosc. Radiat. Transf. 177 (2016) 75–91, https://doi.org/10.1016/J.JQSRT.2016.01.024.
[47] R.H. Dicke, The effect of collisions upon the Doppler width of spectral lines, Phys. Rev. 89 (1953) 472, https://doi.org/10.1103/PhysRev.89.472.
[48] V.G. Cooper, A.D. May, B.K. Gupta, Interferometric measurement of line widths and frequencies of the s 0 (0) and s 0 (l) rotational Raman lines of h 2, Can. J. Phys. 48 (1970) 725–729, https://doi.org/10.1139/p70-090.
[49] V.G. Cooper, A.D. May, E.H. Hara, H.F.P. Knapp, Dicke narrowing and collisional broadening of the S0(0) and S0(1) Raman line of H2 46 (2011) 2019–2023, https://doi.org/10.1139/P68-547.
[50] M.N. Polyanskiy, Refractiveindex.info database of optical constants, Sci. Data 11 (2024) 1–19, https://doi.org/10.1038/s41597-023-02898-2.
[51] K.K. Wong, Properties of Lithium Niobate, INSPEC/Institution of Electrical Engineers, 2002.
[52] D. Sun, Y. Zhang, D. Wang, W. Song, X. Liu, J. Pang, D. Geng, Y. Sang, H. Liu, Microstructure and domain engineering of lithium niobate crystal films for integrated photonic applications, Light Sci. Appl. 2020 9 (2020) 1–18, https://doi.org/10.1038/s41377-020-00434-0.
[53] J.C. Joshi, A.L. Dawar, Pyroelectric materials, their properties and applications, Phys. Status Solidi 70 (1982) 353–369, https://doi.org/10.1002/PSSA.2210700202.
[54] M. Gonzalez, H. Seren, E. Buzi, M. Deffenbaugh, Fast downhole fluid viscosity and density measurements using a self-oscillating tuning fork device, SAS 2017 - 2017, IEEE Sens. Appl. Symp. Proc. (2017), https://doi.org/10.1109/SAS.2017.7894045.
[55] M. Giglio, P. Patimisco, A. Sampaolo, G. Scamarcio, F.K. Tittel, V. Spagnolo, Allan deviation plot as a tool for Quartz-Enhanced photoacoustic sensors noise analysis, IEEE Trans. Ultrason. Ferroelectr. Freq. Control 63 (2016) 555–560, https://doi.org/10.1109/TUFFC.2015.2495013.
[56] M. Matejcek, M. Sostronek, Computation and evaluation allan variance results, NTSP 2016 - proc. Int. conf, N. Trends Signal Process (2016), https://doi.org/10.1109/NTSP.2016.7747786.
[57] W.J. Riley, Handbook of Frequency Stability Analysis, NIST National Institute of Standards and Technology, 1994.
[58] M. Vágner, P. Beneš, Z. Havránek, Experience with allan variance method for MEMS gyroscope performance characterization, 2012, IEEE I2MTC - Int. Instrum. Meas. Technol. Conf. Proc, 2012, pp. 1343–1347, https://doi.org/10.1109/I2MTC.2012.6229362.

Mariagrazia Olivieri obtained the M.S. degree (cum laude) in Physics in 2021 from the University of Bari. From the same year, she was a PhD student at the Physics Department of the University of Bari carrying out her research work at PolySense Lab, joint-research laboratory between Technical University of Bari and THORLABS GmbH. Currently, she is a post-doc researcher at PolySense Lab and her research activities are focused on the development of gas sensors based on Quartz Enhanced Photoacoustic spectroscopy for the analysis of complex gas mixtures.

Giansergio Menduni received the M. S. degree (cum laude) in 2017 and the Ph.D. degree in 2021 in Electronic Engineering from the Polytechnic University of Bari. Since 2022, he is an Assistant Professor in Applied Physics at the Physics Department of Polytechnic University of Bari. His research activity is focused on the development of gas sensors based on Quartz-Enhanced Photoacoustic Spectroscopy (QEPAS) and Light-Induced Thermoelastic Spectroscopy (LITES) on the signal conditioning of Quartz Tuning Forks transducers.

Andrea Zifarelli received the M.S. degree (cum laude) in Physics in 2018 from the University of Bari and his Ph.D. in Physics from the University of Bari in 2022. His research activities were mainly focused on the development of spectroscopic techniques based on laser absorption for the analysis of complex gas mixtures by employing quartz tuning forks as sensitive elements. This investigation was performed by using innovative laser sources as well as developing new algorithms for multivariate analysis approaches. Currently, his research activities are carried out at the PolySenSe Lab, joint-research laboratory between Technical University of Bari and THORLABS GmbH.

Aldo F.P. Cantatore received his M.S. degree in Physics (cum laude) in 2022 from the University of Bari. From the same year, he is a Ph.D. student at the Physics Department of the University of Bari, developing his research work at PolySense Lab, joint research laboratory between the Polytechnic of Bari and THORLABS GmbH. His current research activities are mainly focused on the Quartz-Enhanced Photoacoustic Spectroscopy-based analysis of complex gas mixtures, as well as on the development of open-path sensors based on Light-Induced Thermoelastic Spectroscopy.

Marilena Giglio received the M.S. degree (cum laude) in Applied Physics in 2014, and the PhD Degree in Physics in 2018 from the University of Bari. Since 2021, she is an Assistant Professor at the Physics Department of the Technical University of Bari. Her research activity is focused on the development of gas sensors based on Quartz-Enhanced Photoacoustic Spectroscopy and on the optical coupling of hollow-core waveguides with interband- and quantum-cascade lasers.

Huseyin R. Seren received the B.S. and M.S. degrees in electrical engineering from Koç University, Istanbul, Turkey, in 2007 and 2009, respectively, and the Ph.D. degree in mechanical engineering from Boston University, Boston, MA, USA, in 2014, respectively. He is currently a Research Scientist with the Aramco Services Company, Houston, TX, USA. His current research interests include miniaturized sensors for harsh environments, microelectromechanical systems, and electromagnetic metamaterials.

Miguel Gonzalez received the B.S. degree in physics from the Universidad de Los Andes, Bogota, Colombia, in 2005, and the Ph.D. degree in physics from the University of Florida, Gainesville, FL, USA, in 2012. During his Ph.D., he developed MEMS resonators to study the viscous properties of superfluid helium at low and ultralow temperatures. He is currently a Research Scientist with the Sensors Development Team, Aramco Services Company, Houston, TX, USA, where he is focused on novel rheological measurements for oilfield applications. His current research interests include MEMS, NEMS, nonlinear mechanical systems, micro/nanofluidics, and the properties of complex fluids and flows.

Huadan Zheng received his Ph.D. degree in atomic and molecular physics from Shanxi university, China, in 2018. From 2016–2017, he studied as a joint Ph.D. student in the electrical and computer engineering department and rice quantum institute, Rice University, Houston, USA. Currently he is an associate professor in the Department of Optoelectronic Engineering of Jinan University. His research interests include optical sensors and laser spectroscopy techniques.

Hongpeng Wu received his Ph.D. degree in atomic and molecular physics from Shanxi University, China, in 2017. From September, 2015 to October, 2016, he studied as a joint Ph.D. student in the Electrical and Computer Engineering Department and Rice Quantum Institute, Rice University, Houston, USA. Currently he is a professor in the Institute of Laser Spectroscopy of Shanxi University. His research interests include gas sensors, photoacoustic spectroscopy, photothermal spectroscope and laser spectroscopy techniques.

Lei Dong received his Ph.D. degree in optics from Shanxi University, China, in 2007. From June, 2008 to December, 2011, he worked as a post-doctoral fellow in the Electrical and Computer Engineering Department and Rice Quantum Institute, Rice University, Houston, USA. Currently he is a professor in the Institute of Laser Spectroscopy of Shanxi University. His research interests include optical sensors, trace gas detection, photoacoustic spectroscopy and laser spectroscopy.

Pan Luo is a lead geologist in Saudi Aramco Oil Company, working for resource assessment, subsurface challenges, and upstream technology development and deployment. Pan is leading multiple projects in regional charge evaluation and the development of advanced gas sensor and geochemical logging software for real-time and time-lapse measurement and interpretation. Pan got his PhD degree at the Institute of Geology and Geophysics, CAS in 2010.

Pietro Patimisco obtained the Master degree in Physics (cum laude) in 2009 and the PhD Degree in Physics in 2013 from the University of Bari. Since 2018, he is Assistant professor at the Technical University of Bari. Dr. Patimisco's scientific activity addressed the study and applications of trace-gas sensors, such as quartz-enhanced photoacoustic spectroscopy and cavity enhanced absorption spectroscopy in the mid infrared and terahertz spectral region, leading to several publications.

Vincenzo Spagnolo received the degree (summa cum laude) and the PhD, both in physics, from University of Bari. He works as Full Professor of Applied Physics at the Technical University of Bari. In 2019, he became Vice-Rector of the Technical University of Bari, deputy to Technology Transfer. Since 2017, he is the director of the joint-research lab PolySense, created by THORLABS GmbH and Technical University of Bari, devoted to the development and implementation of novel gas sensing techniques and the realization of highly sensitive QEPAS trace gas sensors.

Angelo Sampaolo obtained his Master degree in Physics in 2013 and the PhD Degree in Physics in 2017 from University of Bari. He was an associate researcher in the Laser Science Group at Rice University from 2014 to 2016 and associate researcher at Shanxi University since 2018. Since 2019, he is Assistant Professor at Polytechnic of Bari. His research activity has focused on the development of innovative techniques in trace gas sensing, based on Quartz-Enhanced Photoacoustic Spectroscopy and covering the full spectral range from near-IR to THz.